Turn-On Dynamics of 2D Random Scatterer Lasers
– First Simulation Results –

draft by Ede Wünsche

June 26, 2012

Abstract

The turn-on of lasers with rectangular, circular and ring-shaped excitation spots is compared. The relaxation oscillations of all cases are similar. Steady states are preferently single-moded (rectangle), two-moded (circle), and multi-moded (ring). Latter case is geometry-forced multimode operation.

1 Introduction

During our meeting in Brazil in the first days of April, we agreed to start the project "Lasing networks in semiconductors" with focus on the turn-on dynamics (TD) of random laser (RL) configurations. The TD of semiconductor lasers usually exhibits damped oscillations of intensity and inversion towards a steady state, the so called relaxation oscillations (RO)[1]. Analyzing frequency and damping constant of RO provides important information on the dynamics of the laser. Furthermore, a laser often operates multimode during the RO even when its steady state is single mode. Thus, its TD is governed by and can provide informations on the mode spectrum of the laser. This is the point where we see the connection to random-matrix theory, which could yield mathematical results on the characteristica of mode spectra of classes of random scatterer configurations. In the real RLs available so far [1], shape and positions of the scatterers are fixed by the growth process. Thus, different configurations can be implemented only by changing the pump spot. It could be interesting to compare different sizes and shapes of this spot.

It is useful to complement experiment and mathematical theory by numerical simulations. In this draft, I summarize first numerical results on RLs of the type sketched in Fig. 1. The calculations base on the network model described in [2]. For simplicity, only scattering by isotropic point scatterers is considered here. Thus, the results are limited to weak scattering. The numerics is challenging, some details will given in the Appendix. The subsequent sections present results for three different shapes of the excitation spot: stripe, circular, and ring.

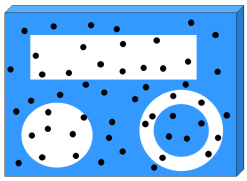

Figure 1: *Scheme of a planar semiconductor waveguide with scatterers (black dots). The white areas illustrate three different types of pump spots. Blue: unpumped, absorbing. Lasing starts, if the amplification between scatterers within a spot compensates the scattering losses.*

How do such lasers turn on? New effects compared to known laser types? No systematic study of such questions is given because the number of possible configurations is endless and only few concrete examples have been calculated. Nevertheless, some conclusions are drawn finally.

Main parameters of all calculations: Central vacuum wavelength $\lambda_0 = 365$ nm. Phase and group velocities $c = c_0/\bar{n}$ with $\bar{n} = 2$. Inversion life time $\tau_n = 500$ ps. Scattering amplitude $A_s = 4i$ (maximum of elastic point-scattering). The corresponding scattering cross section is $\sigma = |A_s|^2\lambda_0/8\pi\bar{n} \approx 116$ nm. With typical scatterer density $\rho \approx 500$ mm^{-2}, the corresponding mean free path of light $l_{\text{free}} \approx 1/(\sigma\rho) \approx 2$ cm is much larger than the spot sizes. This distinguishes the considered configurations from other random lasers (see, e.g., [3, 4, 5]).

[1] Note that the notion "relaxation oscillation" in nonlinear sciences is also used for self-sustaining oscillations with fast-slow dynamics as e.g. the FitzHugh-Nagumo oscillator. In contrast, small-amplitude RO of a laser are harmonic oscillations with decaying amplitude. The steady state of the laser is a focus.

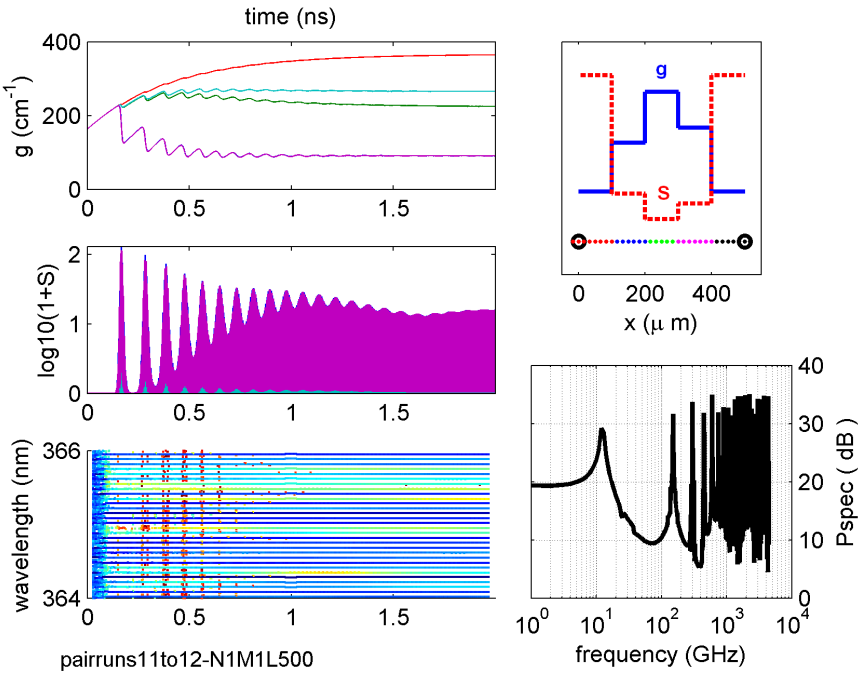

Figure 2: *Turn-on of a pair laser. Left panels: evolution of gain g (top) and mean intensity S (middle) in each domain as well as positions of spectral peaks (bottom). Spectra are calculated with a shifting window of length $2^9 dt \approx 20$ ps. For each window, the positions of spectral peaks are plotted at the centrum of the window. Logarithms of the spectral peak heights are color coded from dark blue = highest peak in the actual window to red = 40 dB below. Lower peaks are disregarded. In order to resolve the closely spaced modes, a reduced spectral interval $\Delta\lambda = 2$ nm is used in this calculation, compared to subsequent cases. Right top: spatial distributions (not to scale) of gain (solid blue) and intensity (dashed red). Below positions of scatterers (circels) and grid points (dots with colors distinguishing between domains). Right bottom: power spectrum.*

2 Reference configuration: the equivalent pair laser (EPL)

In case of weak scattering, the threshold of an RL is governed by the two scatterer with largest separation L [5, 1]. Disregarding all other scatterers yields what I call the equivalent pair laser (EPL). The EPL will serve as a reference for all following RL configurations. In 2D, the EPL threshold is

$$g_{\text{th}}(L) = \frac{1}{L}\ln(\frac{1}{R_{\text{eff}}}) \qquad \text{with effective reflectivity } R_{\text{eff}} = \frac{\sigma}{2\pi L}. \tag{1}$$

The turn-on of a pair laser with $L = 0.5$ mm is pesented in Fig. 2. Its threshold is as high as $g_{\text{th}}(L) = 204$ cm^{-1} due to the extremely small feedback $R_{\text{eff}} \approx 3.7 \times 10^{-5}$. The relative pump rate is $P_{\text{rel}} = 2$, i.e. the unsaturated gain is twice the threshold gain. Initially, the light amplitudes are set to zero. The gain is prebiased to about 80% of the threshold to avoid long turn-on delays.

The gain rises until exceeding threshold and the first spike of the RO evolves. The stimulated emission during the spike depletes the so far homogeneous gain only at the ends of the laser, whereas gain continues growing in the middle. Reason is the extreme amplification along the cavity, $e^{gL} \approx 3 \times 10^4$, which makes high intensities at the two scatterers. The final stationary gain and power distributions are accordingly inhomogeneous. Such large spatial hole burning (SHB) is well known from FP lasers with small reflectivities.

The spectra before spiking are typical for the random spontaneous emission. Thereafter they correspond

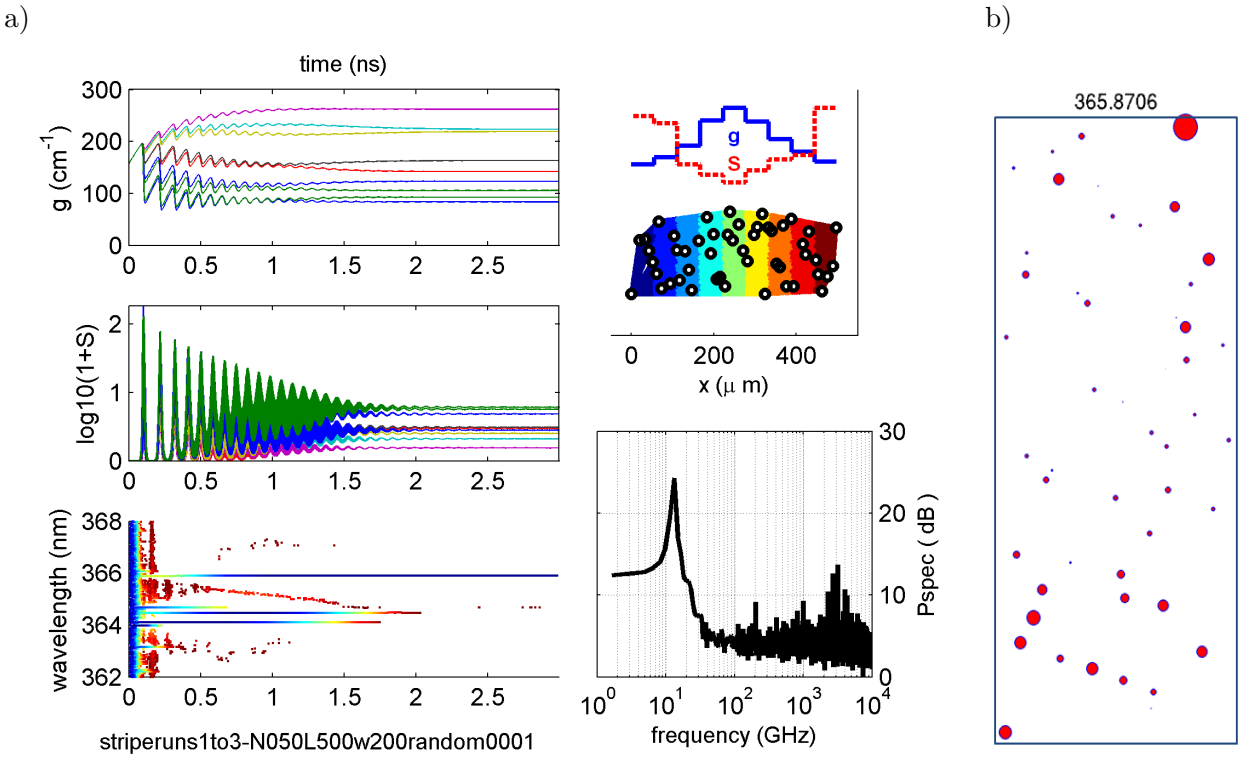

Figure 3: *Stripe excitation. Panels in a) correspond to those in Fig. 2b. b) Top view on the scatterers, circle size proportional to relative intensities at the scatterers in the dominant mode.*

to the known multimode spectra of FP lasers without gain dispersion. Equidistant modes, separated by $\delta\lambda = \lambda_{\text{vak}}^2/2Ln_{\text{group}} = 66.67$ pm. All modes posses the same threshold and should lase with the same intensity. The initial differences seen here are due the fluctuations of initial spontaneous emission. They would average out over epoches much longer than the simulation time 3 ns.

The powerspectra have large contributions from all integer multiples of the round trip frequency and the intensity S shows fast beating oscillations. The long-time limit appears as a steady state only when averaging over the round trip time or longer intervals.

Frequency and damping of the RO are roughly $\nu_{\text{RO}} \approx 12$ GHz and $\Gamma \approx$ 2-3 ns^{-1}. Within the uncertainties, these values compare well with the standard expressions for a single-mode laser,

$$\nu_{\text{RO}} = \frac{1}{2\pi}\sqrt{\frac{P_{\text{rel}}-1}{\tau_p\tau_n}} \approx 12.5 \text{ GHz}, \qquad \Gamma = \frac{P_{\text{rel}}}{2\tau_n} = 2 \text{ ns}^{-1}. \tag{2}$$

with photon life time $\tau_p = (g_{\text{th}}c)^{-1} \approx 1/3$ ps.

3 Stripe Excitation

50 scatterers are randomly distributed within a 0.5 mm $\times$ 0.2 mm stripe[2]. The stripe is pumped at $P_{\text{rel}} = 2$, i.e. the unsaturated gain is twice the EPL threshold (1). The turn-on is similar to the EPL (Fig. 3). The first spike apears a bit earlier, indicating a mode with an slightly reduced threshold. The RO parameters and the amount of SHB are also unchanged. Thus, the stripe laser has not only the same threshold, but also the same RO as its EPL.

[2] 500 scaterers per mm^2, mean distance $\approx 50\mu$m $\approx 60\lambda$.

However, optical spectra evolve differently. Only few modes get dominant (blue). Initially dominant modes switch off and new modes start to lase before single-mode operation is achieved. Obviously, the time scale of this mode competition is much longer than all other time scales. In view the Fig. below, which is redrawn from Ref. [1], these features are easy to understand.

The modal thresholds (dots) of an RL fluctuate around the EPL value (dashed). Modes with low thresholds, i.e. with long decay times, capture most spontaneous emission. Only the mode with lowest threshold survives in a steady state with homogeneous gain. However, the modal thresholds depend on the spatial gain distribution, and get rearranged during the formation of the deep spatial hole, explaining the observed mode exchange.

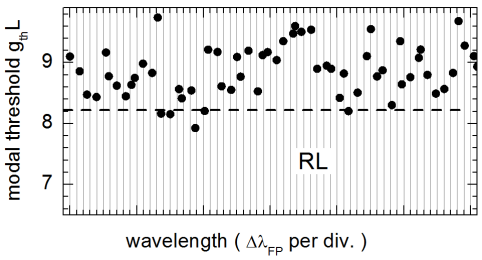

Whereas the overall longitudinal distribution of gain and power shown in panel a) is similar to the EPL, the powers impinging on the individual scatterers (pannel c) exhibit some additional features. As expected, large intensities appear only on scatterers close to the ends of the stripe (cf. panel c). In particular, the scatterer in the right top corner is most intense in agreement with the EPL model. However, not only the two most distant EPL scatterers contribute, but groups of several scatterers close to the respective corners. All they provide feedback, which might explain the observed threshold reduction. But why is this reduction comparably small? Collective feedback helps only, if it is constructive. But the phases of the light fed back from a scatterer group are random. A somehow constructive superposition is possible only for few wavelengths and at some positions.

Following fact is interesting in this context. Dark scatterers appear not only in the middle of the stripe, where the general intensity is small, but also close to the ends, between scatterers with much higher intensities. This strong spatial modulation of the mode field is an effect of the interference pattern between the partial waves reflected from the scatterer group on the opposite end of the stripe. In the depicted mode, the mentioed dark scatterers are sitting in nodes of this pattern. They don't contribute to the feedback. This way, scatterers with destructive feedback phase are perhaps neutralized.

Repeated calculations with few different configurations yielded similar results. Summarizing, the initial spiking and the RO of stripe lasers of randomly distributed weak scatterers are very similar to FP lasers with small reflectivities. They have a stronger tendency to reach single-mode (perhaps sometimes few-mode) emission than an FP laser because – due to randomness – only few modes have low thresholds. The differences between the lowest thresholds within the gain bandwidth is small and varies with time due to SHB, which gives rise to long epoches of mode competition. In experiments, pulsed pumping is often used. If the excitatin pulse is shorter than the formation time of the spatial hole, single-mode operation cannot be expected, even if the stationary case is single-moded.

4 Circular Excitation Spot

Compared to a stripe, circular excitation provides more scatterer pairs with nearly extreme distance $L = 2R$ and these pairs possess different orientations. Thus, a different behaviour might be expected. The particular calculation depicted in Fig. 4 confirms this expectation. 100 scatterers are randomly distributed within a circle with diameter $L = 0.5$ mm. Again, the spot is pumped at twice the EPL threshold, $P_{\text{rel}} = 2$.

The turn-on behaviour and the RO parameters are again similar to that of the EPL. Mutatis mutandis, the intensity distributions are also similar: the intensities in the middle of the circle are smaller than at the circumference, in agreement with the weak-scattering picture – at least in average. Accordingly, the gain is maximum in the center and nearly circular symmetric.

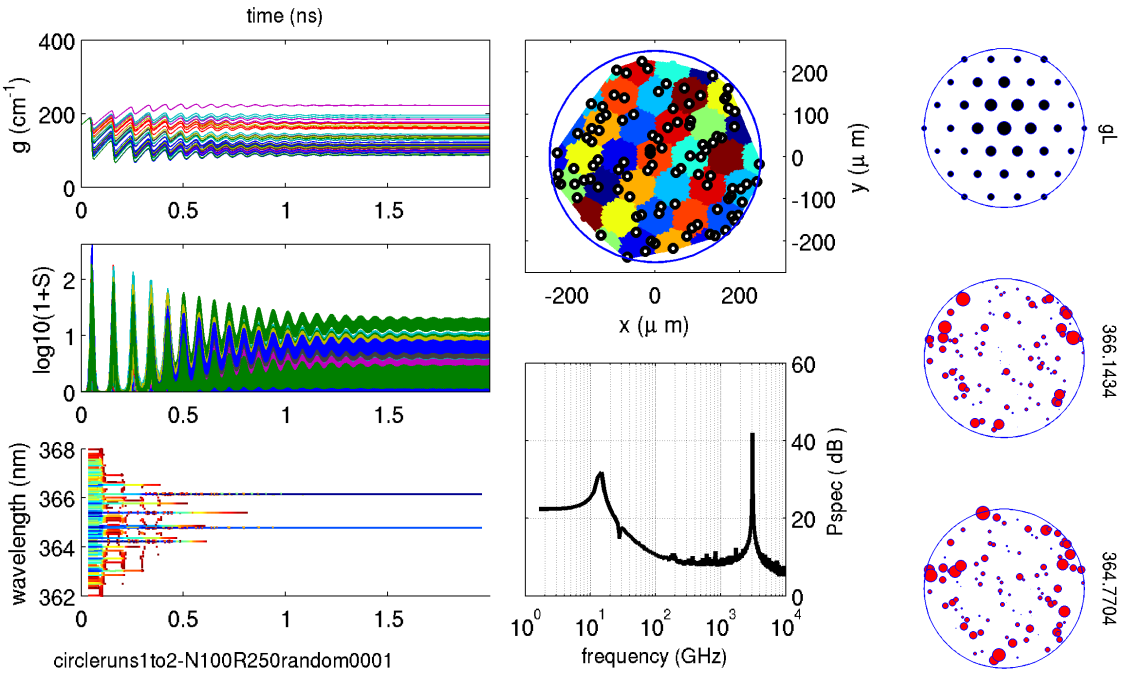

Figure 4: *Circular excitation. Notions as in Fig. 3. Right: spatial distribution of gain in the domains (top circle, the dot size is proportional to g) and modal intensities S at the scatterers (diameter of the circles proportional to intensity) for the two surviving modes (labels: wavelength in nm).*

But, two modes seem to survive now in the steady state. Accordingly, a sharp and strong beating peak close to 3 THz dominates the power spectrum[3]. At first glance, the intensity distributions of the two finally coexisting lasing modes are very similar. However, they are indeed different, which can be seen when looking to the strongest scatterers. This means the modes profit from gain in different spatial regions, which allows them to coexist.

5 Ring-Shaped Excitation Spot

A ring is pumped now with inner and outer radii $R_i = 0.2$ mm and $R_a = 0.25$ mm, respectively. It contains 100 scatterers. The relative pump power is again $P_{\text{rel}} = 2$. However, the absolut pump power is larger than in previous cases, because the EPL threshold is increased (up to 352/cm). Reason is the shorter largest distance of two optically connected scatterers, $L \approx 0.27$ mm.

The turn-on (Fig. 5) is a bit more complex than in the cases considered so far. In particular, the rise of a fourth mode beyond 1 ns causes a reordering of intensities. Finally, four modes coexist. In contrast to previous circular spot, this degeneracy is forced by geometry. Two scatterers in opposite parts of the ring are not directly connected due to the assumed absorption in the interior. The maximum distance between two connected scatterers is limited by $L \leq 2\sqrt{R_a^2 - R_i^2} = 0.3$ mm. This distance is only about $\frac{1}{5}$ of the circumference. The second mode (363.555 nm) corresponds to one such pair. There is still room for a corresponding pair on the other side, the third mode (364.3281 nm). The first mode (365.756 nm) combines four such pairs, slightly rotated.

Interestingly, the modes and the gain pattern (blue dots on top) are redolent of hexagonal symmetry

[3]Two-mode lasers are indeed constituents of some setups for the generation of THz radiation [6].

rather than pentagonal symmetry expected from above consideration. This effect appears also with other scatterer configurations in the ring. It could be interesting to check whether this is occasional and how it is related with the ratio between inner and outer radius of the ring.

Irrespective of the multimode behaviour, the RO frequency is again close to that of the EPL, $\nu_{\mathrm{RO}} \approx 16.3$ GHz according to (2).

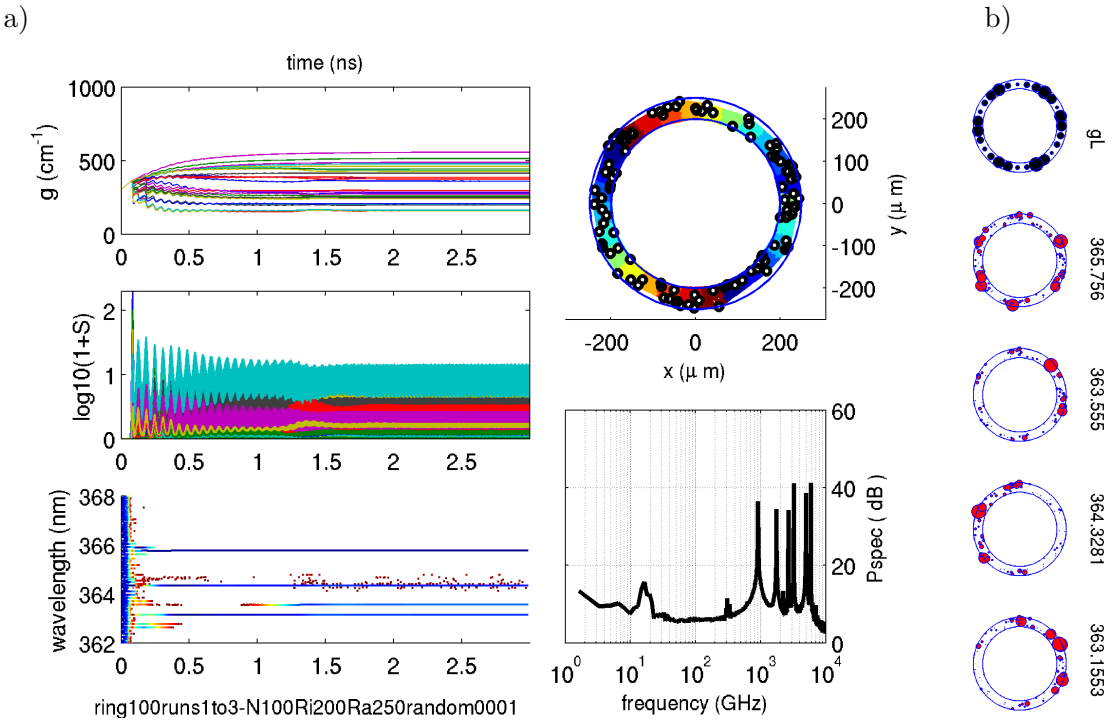

Figure 5: *Ring-shaped excitation spot. Notion as in Fig. 4. a) Turn-on dynamics. c) Final distribution of g in the domains (top) and of the intensities at scatterers for the final modes (decreasing intensity from top to bottom, right labels: wavelength in nm).*

6 Conclusions, problems, outlook

- Independent of the geometry of the excitation spot, the threshold and the characteristica of the relaxation oscillations are well approximated by the equivalent pair laser. With respect to these quantities, we cannot expect big surprizes.
- The time scale of mode dynamics is much longer than all the other ones. It is in the range of nanoseconds. When exciting with ns-pulses, we cannot expect to reach mode equilibrium.
- For longer times, stripe geometry tends towards single mode operation, whereas circular and ring-shaped excitation spots yielded multimode operation.
- These results are limited to a fixed parameter set, in particular $\alpha_H = 0$ (no amplitude-phase coupling, which is known to cause dynamic instabilities), $P_{\mathrm{rel}} = 2$ (higher pump rates may cause more pronounced spatial hole burning), weak isotropic scattering (stronger scatterers can perhaps better support multimode operation). Studies of these parameters are required. A first shot on the impact of α_H is given in Appendix B.

References

[1] S. Kalusniak, H.-J. Wünsche, and F. Henneberger, *Random Semiconductor Lasers: Scattered versus Fabry-Perot Feedback*, Phys. Rev. Lett. **106**, 013901 (2011)

[2] H.-J. Wünsche, *A Model for the Dynamics of Semiconductor Scatterer Lasers*, March 1, 2012. (draft, http://people.physik.hu-berlin.de/ ede/sld/sld8.pdf)

[3] D.S. Wiersma, *The physics and applications of random lasers*, Nature Physics **4**, 359 (2008).

[4] O. Zaitsev and L. Deych, *Recent developments in the theory of multimode random lasers*, J. Opt. **12**, 024001 (2010).

[5] X. Wu et al., *Random lasing in weakly scattering systems*, Phys. Rev. A **74**, 053812 (2006).

[6] Masahiko Tani, Osamu Morikawa, Shuji Matsuura, and Masanori Hangyo, *Generation of terahertz radiation by photomixing with dual- and multiple-mode lasers*, Semicond. Sci. Technol. 20 (2005), S151-S163

Appendix

A Numerical model

The model bases on [2] but takes a slightly different point of view and introduces additional approximations. I shall give a brief summary of the underlying ideas and equations followed by a description of the numerical implementation.

A.1 model ideas and equations

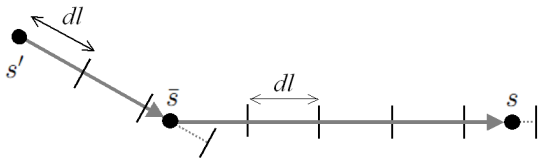

The graphics illustrates the optical components of the model. Basic constituents are *scatterers* (here $s', \bar{s}, s$) and *rays* (labeled by index r) – the directed paths from one scatterer to another one. With N_s scatterers, there are $N_r = 2N_s(N_s-1)$ rays. $N_s - 1$ other rays arrive at each ray r. Furthermore, the pumped area is appropriately partitioned into domains d. Spatially constant gain $g_d(t)$ is assumed in each domain.

The optical amplitude of the light traveling along a ray r is

$$E_r(z,t) = \mathcal{E}_r(z,t)G(k,z)e^{-i\omega_0 t} + \text{c.c.}, \tag{3}$$

where z is the distance on the ray. The far-field 2D Green function $G(k,r) = \exp(ikr + i\pi/4)/\sqrt{8\pi kr}$ describes amplification and phase shift of the wave according to a constant complex reference wave number $k = 2\pi\bar{n}/\lambda - i(\bar{g} - \alpha_0)/2$ ($\bar{n}, \bar{g}, \alpha_0$: reference values of refractive index, gain, background losses).

Slow amplitude and gain obey the set of equations

$$(\partial_z + \frac{1}{c}\partial_t)\mathcal{E}_r(z,t) = \left[\frac{1-i\alpha_H}{2}(g(z,t) - \bar{g}) - \frac{\alpha_0}{2}\right]\mathcal{E}_r(z,t) \qquad \text{where } g(z,t) = g_d(t) \text{ if} z \in d, \tag{4}$$

$$\tau_n \frac{d}{dt} g_d(t) = g_0 - g_d(t)\left[1 + S_d(t)\right], \tag{5}$$

where $S_d(t)$ is the average intensity in domain d. Scattering enters via the boundary conditions

$$\mathcal{E}_r(0,t) = \sum_{r' \in r_{\text{in}}(r)} A_{rr'}\left[\mathcal{E}_{r'}(l',t)G(k,l') + \beta_{\text{spont}}\right] \tag{6}$$

The r'-sum goes over all rays arriving at r. l' denotes their lengths and β_{spont} is a small Langevin force simulating spontaneous emission impinging on the scatterers from everywhere. $A_{rr'}$ is the scattering amplitude from ray r into ray r'. In present study, I used $A_{rr'} = 4i$, which supposes scatterers small compared to wavelength and scatterer separation. The Mie-scattering approach of Ref. [1] is a better approximation, holding as long as the seperation between scatterers is large compared to scatterer size and wavelength. In general, it is always a certain matrix.

A.2 numerical implementation

To calculate spectral dynamics within a given spectral interval $\Delta\lambda$ (6 nm), centered at a wavelength λ_0 (365 nm), a time step $dt = \frac{\lambda_0^2}{2c_0\Delta\lambda}$ (37 fs) is used. It yields the space step $dl = cdt$ (5.5 μm) for

discretizing on each ray. The last grid point of the ray is taken just beyond or at the final scatterer. On the grid, the field is represented by logarithmic amplitudes

$$\psi = \ln(\mathcal{E}(z,t)) \tag{7}$$

for numerical efficiency. The ψ of all rays are put sequently into a large one-dimensional array (4×10^5 elements for the circular excitation).

In each time step, ψ and g_d are updated in sequence. The update of ψ is done in two subsequent steps. First, I propagate the field according to (4) one step along the rays

$$\psi(z,t) = \psi(z - dl, t - dt) + \frac{1}{2}\left[(1 - i\alpha_H)(g_{d(z-dl)}(t) - \bar{g}) - \alpha_0\right] dl. \tag{8}$$

This propagation step is most time consuming. I found best performance when exploiting the matlab operation CIRCSHIFT, which shifts the components of an array circularly. This gives wrong in-values on each ray, which in a second step are set according to

$$\psi_r^{\mathsf{in}} = \ln(\mathcal{E}_r^{\mathsf{in}}), \quad \text{where} \quad \mathcal{E}_r^{\mathsf{in}}(t) = \sum_{r' \in r_{\mathsf{in}}(r)} A_{rr'} \left[\mathcal{E}_{r'}^{out}(t) G(k, l') + \beta_{\mathsf{spont}}\right] \tag{9}$$

are the fields injected into ray r by the instantaneous scattering. The r'-sum goes over all rays arriving at r. l' denotes their lengths and β_{spont} is a small complex random number simulating spontaneous emission impinging on the scatterers from everywhere. $\mathcal{E}_{r'}^{out}(t) = \exp(\psi_{r'}^{out}(t))$ denotes the smooth field amplitude on the final scatterer of ray r'. Since in general this scatterer sits between the two last grid points (see figure), this amplitude is not exactly available but is determined by linear interpolation. This approximation introduces an artificial numeric dispersion that supresses high-frequency modes. I didn't find a way to better treat this problem. Fortunately, this numeric dispersion can be used to simulate the real gain dispersion, which is limiting the amplification band width.

Now, the gain g is updated. It is given on the independent spatial domain-grid. The temporal grid for g_d is shifted by $dt/2$ compared to the grid of $\mathcal{E}$. Accordingly, the simplest integration of the rate equations (5) over one interval dt yields the update formula

$$g_d(t + \frac{dt}{2}) = g_d(t - \frac{dt}{2}) + \left[g_0 - g_d(t - \frac{dt}{2})(1 + S_d(t))\right] \frac{dt}{\tau_n}. \tag{10}$$

The mean intensity S_d in the domain is estimated as the average over the impinging intensities at all scatterers in the domain, symbolically

$$S_d = \langle |E_s|^2 \rangle_{s \in d}. \tag{11}$$

Note, the E_s contain the Green function G in contrast to the prefactor $\mathcal{E}$.

The described numerical approach is programmed with Matlab. The largest example (100-scatterer circle) required about 100 minutes runtime for 1 ns (about 27000 time steps dt) on a Dell PowerEdge T710.

A.3 Evaluation of calculated data

The gain $g_d(t)$ of the domains and the total amplitudes

$$\mathcal{E}_s^{\mathsf{in}}(t) = \sum_{r' \to s} \mathcal{E}_r(l', t) G(k, l') \qquad \text{(sum over all rays pointing to scatterer } s\text{)} \tag{12}$$

impinging on the scatterers are saved in a file trace.mat. The figures presented are drawn from these raw data in a postprocessing step. The plot of g and S is evident. Spectral dynamics has been explained in the caption of Fig. 2. The powerspectrum is obtained from the last 2^{14} steps (0.6 ns) of the time trace. The spatial modal intensity distributions are obtained as follows. First, the optical spectra of all E_s are calculated. The up to 6 highest peaks of the sum of all spectra are determined. Each peaks position λ_m represents a mode. $|E_s(\lambda_m)|^2$ is proportinal to the intensity of mode λ_m at scatterer s and is transferred to the size of the plotted circle.

B First exploration of amplitude-phase coupling

This calculation has been performed for the ring configuration of Fig. 5. The three panels correspond to the left panels of Fig. 5. Every two ns, the value of $-\alpha_H$ has been increased by 1. Obviously, this changes the modes and may cause instabilities. A systematics is beyond present scope.